Journal of Imaging Science and Technology® 66(4): 040415-1–040415-7, 2022.

Segmentation as Domain Knowledge in GAN for Low-dose CT Denoising

Zhi Yin and Zong Zheng
School of Science, Ningbo University of Technology, Ningbo 315016, Zhejiang, China
E-mail: yz@nbut.edu.cn

Abstract. *Low-dose computed tomography (LDCT) denoising is an important topic in medical imaging field. In practice, we aim to preserve the LDCT quality and diagnostic performance while lowering the CT radiation dose. Deep learning-based algorithms such as the convolutional neural network (CNN) and the generative adversarial network (GAN) have recently shown promising results in LDCT denoising. However, limited domain knowledge makes it hard to improve the denoising performance. Instead of manually extracting domain knowledge, we offer a new LDCT denoising scheme and a novel GAN architecture that uses segmentation information as domain knowledge. We demonstrate that domain knowledge from mask LDCT images may be transferred to our denoising GAN for improved LDCT denoising performance. We show that the more precise our semantic segmentation model is, the better our GAN denoising performance is. Furthermore, we posit that the domain knowledge provided by segmentation can come from different datasets, which we refer to as coarse-grained domain knowledge sharing.*
[DOI: 10.2352/J.ImagingSci.Technol.2022.66.4.040415]

1. INTRODUCTION

Low-dose CT (LDCT) denoising is critical since the reduction of the CT radiation dose keep patients safer while compromising image quality. The many methods for LDCT denoising have been proposed in Refs. [1–5].

Recently, deep learning based algorithms such as convolutional neural network (CNN) and generative adversarial network (GAN) have been achieved good performance in industrial applications [6, 7], Internet of Things (IoT) [8–10], medical imaging [11, 12], etc, especially LDCT denoising [13–19]. However in the medical imaging field, it is often hard to improve the performance of the deep learning based methods to clinical level without domain information. Furthermore, it is often hard to transfer the domain rules into denoising process effectively.

Semantic segmentation is a useful technique for categorizing each pixel in an image into one of a number of categories [20]. In the medical imaging scenario, this kind of semantic information can be treated as domain knowledge.

We aim to solve LDCT denoising issue more effectively and automatically, using a combination of GAN architecture [21, 22] and the domain knowledge extracted from semantic segmentation. We assume that the segmentation process is a domain knowledge extraction process. We use tissue semantic segmentation networks with labeled tissue mask information in lung CT. We conclude that the trained segmentation network retains information about the delicate tissue semantic information. In the meantime, inspired by image-to-image translation, we construct a paired cycle-GAN structure [23] in which we also add segmentation network structure. We show that the segmentation information to our network can get better performances on LDCT denoising task. We demonstrated that better semantic segmentation model makes better denoising performance. Moreover, we determined that the dataset for segmentation and dataset in LDCT denoising can be different. In summary, the contributions of this paper are as follows:

- We present a denoising GAN with segmentation network structure and semantic segmentation information for LDCT denoising and show that the segmentation information as domain knowledge can be transferred from mask NDCT images to our denoising GAN to get a better performance on LDCT denoising task.
- We demonstrate the relations between semantic segmentation accuracy and denoising performance. The more accurate our semantic segmentation model is, the better denoising GAN performance is.
- Since the dataset used for semantic segmentation is different from the dataset used for denoising and they are from the same domain (lung CT images), we posit that this kind of domain knowledge is shareable.

2. RELATED WORK

2.1 *Denoising for LDCT Based on CNNs*

Noise reduction for LDCT is a challenging task in medical imaging field. Although there are various methods to tackle it, we focus on the image post-processing technique. Recently, various denoising models based on CNNs have achieved good performance.

CNNs as a deep learning based model can learn the pattern of images. Many CNN based denoising models with different network architectures were proposed. Chen et al. [24] used a 2D CNN to map LDCT images towards its corresponding NDCT counterparts in a patch-by-patch fashion. Wolterink et al. [14] used a GAN for noise reduction in LDCT. Chen et al. [13] handled the LDCT denoising with a residual encoder–decoder CNN. On the other hand, object

Received Dec. 9, 2021; accepted for publication May 15, 2022; published online June 29, 2022. Associate Editor: Ping Wang.
1062-3701/2022/66(4)/040415/7/$25.00

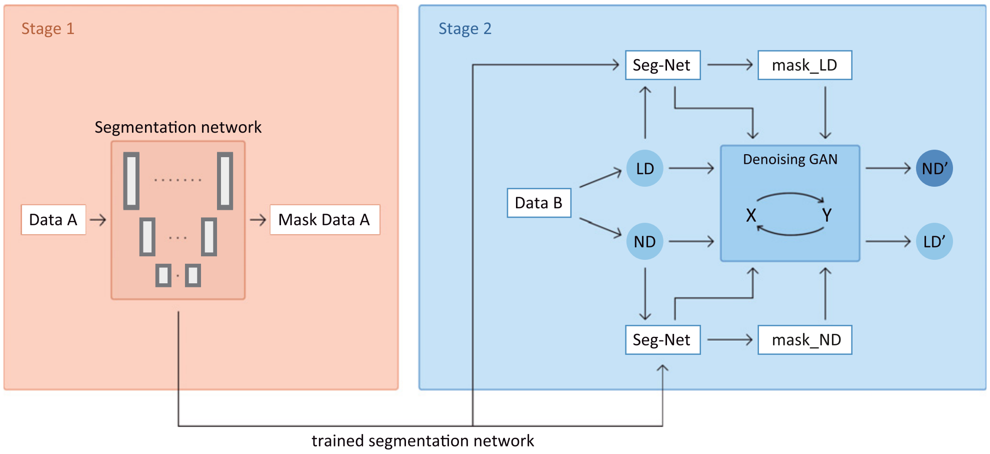

Figure 1. Illustration of the general denoising scheme. *LD*, *ND*, *maskLD* and *maskND* denote low-dose CT dataset, normal-dose CT dataset, segmented low-dose CT images and segmented normal-dose CT images respectively.

functions determine the learning strategy of the model. We can also find many kinds of object functions in CNNs based denoising model such as the mean squared error loss [13, 14, 24], the adversarial loss [14–17] and the perceptual loss [15].

Although we have utilized many CNNs based models for LDCT denoising, the domain knowledge is critical for LDCT denoising. Extracting domain knowledge as experts' rules is an option, however in our work we will transfer the domain knowledge from automatic semantic segmentation.

2.2 *GANs for Image-to-Image Translation*

GANs are a new kind of deep learning paradigm. Recently, more and more GANs were proposed especially in the field of image-to-image translation [23, 25, 26]. From the perspective of whether the training images are paired or not, image-to-image translation can be categorized into two kinds: (i) paired image-to-image translation; (ii) unpaired image-to-image translation.

In the paired image-to-image translation situation, we have both input images and corresponding output images. The training images are paired and we can leverage the information from the paired images from each other.

Because of the scarcity of the paired training images in real life, unpaired image-to-image translation was proposed and the scenarios are more extensive. Zhu et al. [25] present an approach for learning to translate an image from a source domain X to a target domain Y in the absence of paired examples using cycle-consistent adversarial networks. Kim et al. [26] also propose a method based on generative adversarial networks that learns to discover relations given unpaired data between different domains (DiscoGAN).

Although in the scenario of LDCT denoising, it is expensive to find the paired training images (LDCT images and corresponding normal-dose CT (NDCT) images), we will utilize the synthesize data to leverage both pair and unpaired image-to-image translation in our method.

2.3 *Medical Image Segmentation*

Semantic image segmentation is the task of classifying each pixel in an image from a predefined set of classes [20, 27, 28]. In practice, labeling the pixel and segmenting the organs or lesions are expensive and time consuming. However, we can get the domain knowledge at pixel level such as the edge of the lesions or the shape of the tissues, etc. Thus semantic segmentation was used broadly in the medical imaging fields.

Ronneberger et al. [29] presented a convolutional network called U-Net for biomedical image segmentation, which has been successfully applied on medical image segmentation task.

Azad et al. [30] proposed an extension of U-Net, Bi-directional ConvLSTM U-Net with densely connected convolutions (BCDU-Net) for medical image segmentation and achieved state-of-the-art performance on three different kinds of medical image datasets.

As we can see, semantic segmentation models can reflect pixel level domain information, we can utilize it as a domain knowledge extractor.

3. METHODOLOGY

Our goal is to denoise the LDCT images. Although there are lots of CT denoising work with GAN structures, we focus on the effectiveness of the domain information transferred from segmentation and its enhancement for our denoising GAN architecture. First we will propose our general denoising scheme which involves two stages. Then we will describe our denoising GAN in detail, including: the loss of our network, the architecture of it, etc. In the last part of this section, we describe the implementation details of our denoising GAN.

3.1 *General Denoising Scheme*

The general denoising scheme is depicted in Figure 1. We utilize two datasets: Data A is a dataset for domain knowledge extraction with segmentation network. Data B is a dataset which is totally different from Data A and we use it for denoising and evaluation of our method. Data B is originally

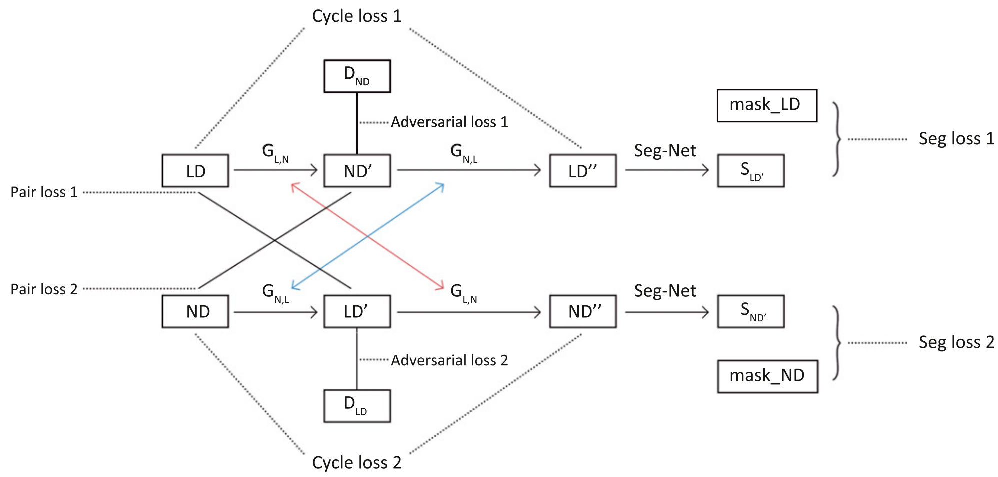

Figure 2. Overview of the proposed denoising GAN. Here, *LD*, *ND*, *maskLD* and *maskND* denote low-dose CT dataset, normal-dose CT dataset, segmented low-dose CT images and segmented normal-dose CT images respectively. S(*LD″*) and S(*ND″*) are short for Seg(*LD″*) and Seg(*ND″*) respectively. The various losses in the diagram will be defined in the next subsection.

a normal-dose CT dataset. For our network training and evaluation target, we synthesis a LDCT dataset called LD from the original Data B. Here, we call the original Data B as NDCT images and the synthesis version which simulated the noisy situation as LDCT images. Data A and Data B are both from the same medical domain and they are both lung CT scan images. However, Data A has semantic segmentation mask, so we can treat it as a labeled domain knowledge source. While Data B prepared now is a paired data source, there are LDCT and NDCT parts in it. So we can utilize the pair information from Data B and evaluate our denoising performance on it.

We divide the scheme into two stages. In Stage 1, we train a semantic segmentation network with the data A and get a trained network. In Stage 2, we propose our denoising network mainly based on a denoising GAN structure. We can fully use the paired lung CT scans in Data B and the segmentation information from Data A. Since there are two kinds of inputs in Data B, namely LDCT and NDCT, we can use segmentation knowledge from Data A to get *maskLD* and *maskND*. Then we set LDCT and NDCT as input of our denoising GAN simultaneously. We make the segmentation structure in our GAN with no prior weights. We train it with the whole denoising GAN. We add the mask LDCT and mask NDCT as the ground truth for one kind of discriminator in our GAN. After the training process stabilized we can get ND' (i.e. the LDCT after denoising) as one of the output of our denoising GAN.

3.2 *Denoising GAN Architecture*

Our goal is denosing the LDCT images and the main part of the denoising process is the denoising GAN. We illustrate the denoising GAN architecture in Figure 2.

We set LD and ND as input of our GAN. They go through the generator $tt_{L,N}$ and $tt_{N,L}$. We can get a pair of generated images ND' and LD'. Then, we continually put ND' and LD' into the generator. Finally, we can get ND'' and LD''. They can form cycle loss with ND and LD. Here, the red line and blue line in the picture means the weights sharing.

Next, we take advantage of the power of segmentation network. We put ND'' and LD'' through a segmentation net and get the corresponding mask images. We use the trained segmentation network and infer the LD and ND. This will form the Seg Loss in our objective functions.

All in all, the total architecture of our denoising GAN is an image-to-image translation structure with segmentation network providing fine grained domain information.

3.3 *Overall Optimization Objective*

Our network architecture is similar to an image-to-image translation network structure. However, we want to transfer the segmentation information and the segmentation network ability. So there are four kinds of loss functions in our network.

3.3.1 *Adversarial loss*

As in Fig. 2, we can see that there is an adversarial loss to the mapping functions. We express the objective as below. Here, all the E denote the expectations from the corresponding data distributions.

$$L_{GAN}(G_{L,N}, D_{ND}, LD, ND) = E_{ND\sim P_{\text{data}}(ND)}[\log D_{ND}(ND)] + E_{LD\sim P_{\text{data}}(LD)}[\log(1 - D_{ND}(G_{L,N}))] \tag{1}$$

and the counterparts objective is:

$$L_{GAN}(G_{N,L}, D_{LD}, ND, LD) = E_{LD\sim P_{\text{data}}(LD)}[\log D_{LD}(ND)] + E_{ND\sim P_{\text{data}}(ND)}[\log(1 - D_{LD}(G_{N,L}))]. \tag{2}$$

Since our network acts as a paired cycle GAN style, we can express the adversarial loss as:

$$L_{GAN}(G, D_y, x, y) = L_{GAN}(G_{L,N}, D_{ND}, LD, ND) + L_{GAN}(G_{N,L}, D_{LD}, ND, LD). \tag{3}$$

3.3.2 *Cycle loss*

In continuation, we introduce the cycle loss. The cycle loss 1 here is the difference between LD and LD'' and the cycle loss 2 is alike. The cycle loss here is for cycle consistency. We ensure that LD and LD'' which pass through the generator are kept consistent. The cycle loss here is expressed as:

$$L_{cyc}(G_{L,N}, G_{N,L}) = E_{LD\sim P_{\text{data}}(LD)}[\|G_{N,L}(G_{L,N}(LD)) - LD\|_1] + E_{ND\sim P_{\text{data}}(ND)}[\|G_{N,L}(G_{L,N}(ND)) - ND\|_1]. \quad (4)$$

3.3.3 *Pair loss*

Since we want to stabilize the network and simultaneously take advantage of the pairing information, we can use the pairing information from real LD and ND. We just need to take the MSE-like style as the loss:

$$L_{\text{par}}(G_{L,N}, G_{N,L}) = E_{LD\sim P_{\text{data}(LD)}}[\|G_{L,N}(LD) - ND\|_1] + E_{ND\sim P_{\text{data}(ND)}}[\|G_{L,N}(ND) - LD\|_1]. \quad (5)$$

3.3.4 *Seg loss*

Finally, since we use the segmentation information as our domain knowledge for denoising. We add a seg loss here which measure the misdistance from segmentation. As shown in Fig. 2, mask_{LD} and mask_{ND} are referenced ground truth of the seg loss while $\text{Seg}(LD'')$ and $\text{Seg}(ND'')$ are the outputs of the denoising GAN structure. We can express it as:

$$ND' = G_{L,N}(LD), \quad LD'' = G_{N,L}(G_{L,N}(LD)) \quad (6)$$

$$LD' = G_{N,L}(ND), \quad ND'' = G_{L,N}(G_{N,L}(ND)) \quad (7)$$

$$\begin{aligned} L_{\text{Seg}}&(\text{Seg}, LD'', \text{mask}_{LD}) \\ &= E_{LD''\sim P_{\text{data}(LD'')}}[\text{mask}_{LD} * \log(\text{Seg}(LD''))] \\ &\quad + E_{LD''\sim P_{\text{data}(LD'')}} \\ &\quad [(1 - \text{mask}_{LD}) * \log(1 - \text{Seg}(LD''))] \end{aligned} \quad (8)$$

$$\begin{aligned} L_{\text{Seg}}&(\text{Seg}, ND'', \text{mask}_{ND}) \\ &= E_{ND''\sim P_{\text{data}(ND'')}}[\text{mask}_{ND} * \log(\text{Seg}(ND''))] \\ &\quad + E_{ND''\sim P_{\text{data}(ND'')}} \\ &\quad [(1 - \text{mask}_{ND}) * \log(1 - \text{Seg}(ND''))] \end{aligned} \quad (9)$$

$$\begin{aligned} L_{\text{seg}}(\text{Seg}) &= L_{\text{Seg}}(\text{Seg}, LD'', \text{mask}_{LD}) \\ &\quad + L_{\text{Seg}}(\text{Seg}, ND'', \text{mask}_{ND}). \end{aligned} \quad (10)$$

So all in all, we can get the full objective of our network as below. It is worth mentioning that various hyperparameters λ here are to balance different losses.

$$\text{Loss} = \lambda_d * L_{\text{GAN}} + \lambda_c * L_{\text{cyc}} + \lambda_p * L_{\text{par}} + \lambda_S * L_{\text{seg}}. \quad (11)$$

4. EXPERIMENTS

4.1 *Datasets*

In our experiments, we choose two datasets: (i) Data A is from a data competition dataset for lung segmentation [31]. We use it for our segmentation task in Stage 1. There are 267 lung CT images and corresponding mask images. (ii) Data B is from another data competition called data science bowl 2017 [32]. As illustrated in Fig. 1, Data A is pretrained for transferring the segmentation information.

Data B is for our denoising task and we use the 1043 images from Data B as a pairing dataset. For training the segmentation and GAN structure simultaneously, we randomly choose 1043 lung CT images from 25 patients in Data B. We take 847 images as train data and 196 images as test data. Image noise comes from various mechanisms, photons hitting, for instance and the behavior of photons hitting the detector are usually treated as Poisson distribution. Also, the electrical noise takes an important role in low-dose CT and is normally a Gaussian distribution [33]. Based on this principle, we take the origin data as NDCT and by adding Poisson and Gaussian noise, we treat the simulated version as LDCT which is our denoising objective.

4.2 *Networking Settings*

In the previous section, we proposed the whole general scheme of our methods and the main architecture of the denosing GANs. To confirm the effectiveness of our methods, we choose two kinds of segmentation network and two kinds of denoising GANs. The segmentation networks chosen are U-Net [29] and LSTM-U-Net [30]. We can find that different segmentation network contribute differently for denoising.

The main part of denoising GANs inspired by Cycle-GAN [23]. So here we use CycleGAN and DiscoGAN [26] as the main part of our denoising GAN. Notably, we fully use the pairing information and segmentation information in our GAN.

4.3 *Parameter Settings*

The segmentation network and denoising GANs in our experiments are all implemented in Keras [34] and Tensor-Flow [35]. We perform our experiments on Nvidia Tesla M40 with 12GB memory to accelerate the training and inference procedure. In our experiments, the learning rate, and batch size are 0.005, and 8 respectively. We chose 100 epochs for training process.

4.4 *Evaluation*

Since our target is to denoise LDCT images, we chose PSNR and SSIM as our metrics. Peak signal to noise ratio (PSNR) and structured similarity index (SSIM) are both chosen for quantitative assessment of image quality. These two metrics are all pixel-level similarity metrics. PSNR is a more objective index for image quality while SSIM focuses more on the structure and the sharpness of the images. So we can evaluate the denoising performance both from objective values and subjective feelings.

5. RESULTS

5.1 *Segmentation as Domain Knowledge*

We set six setups for evaluating our methods. We can see from Table I, the denoising GANs with segmentation perform better than GANs without segmentation in both metrics. Furthermore, we can find that the segmentation

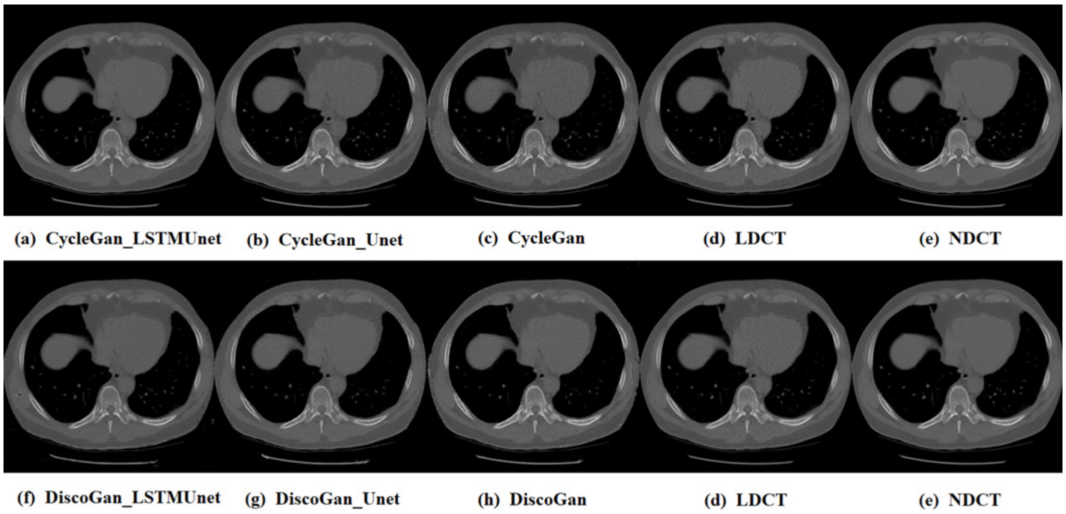

Figure 3. Images with different settings of our denoising GAN.

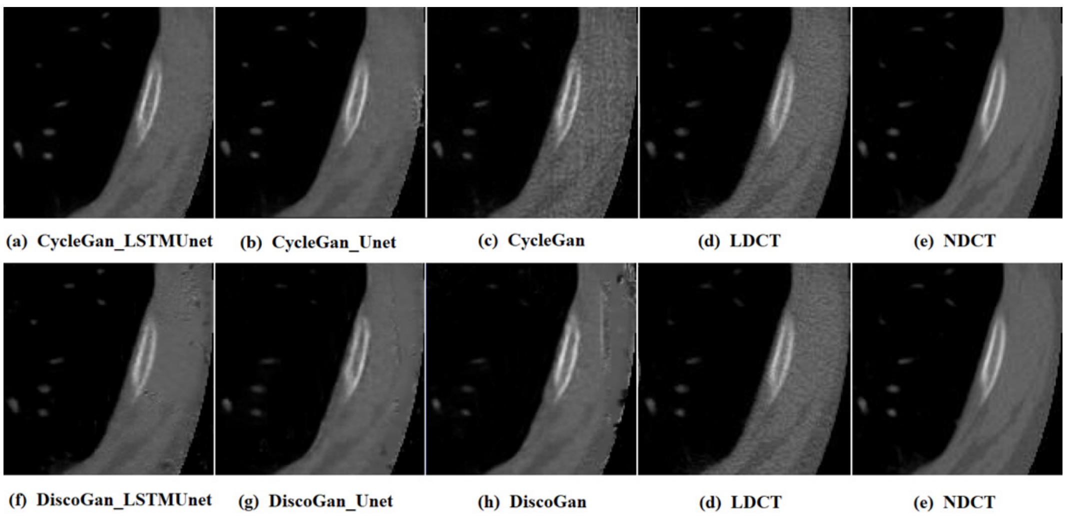

Figure 4. Local details of images with different settings of our denoising GAN.

performance of the segmentation part influence denoising effect. The more accurate the segmentation is, the better the denoising effect. Since LSTMUnet has the best segmentation performance, CycleLSTMUnet has the best denoising effect here, and original LDCT has the lowest value in both metrics.

In Table I, CycleLSTMUnet means that the denoising GAN structure is similar to CycleGAN [23] and the segmentation part is LSTMUnet [30]. CycleUnet means that the denosing GAN structure is similar to CycleGAN and the segmentation part is original Unet structure [29]. Cycle means that there is only CycleGAN structure in the denoising GAN. DiscoUnet means that the denosing GAN structure is similar to DiscoGAN [26] and the segmentation part is Unet structure. Disco means that there is only DiscoGAN structure in the denoising GAN. In last column of Table I, LDCT means the PSNR and SSIM values from the original low-dose CT images. We can find that

Table I. Quantitative results of denoising GANs with and without segmentation information.

	CycleLSTMUnet	CycleUnet	Cycle	DiscoUnet	Disco	LDCT
PSNR	29.347	28.928	27.869	27.363	26.637	25.593
SSIM	0.897	0.887	0.862	0.885	0.858	0.792

Moreover, not only the numeric values of the metrics support our assumption, we can also get the subjective feeling from the denoising images. As we can see from Figures 3 and 4, results of denoising GAN with segmentation information can get smoother edges. Apparently, this kind of images with smoother edges can be more friendly to clinical diagnosis.

Since our segmentation networks are usually for semantic segmentation tasks. We can get the pixel level

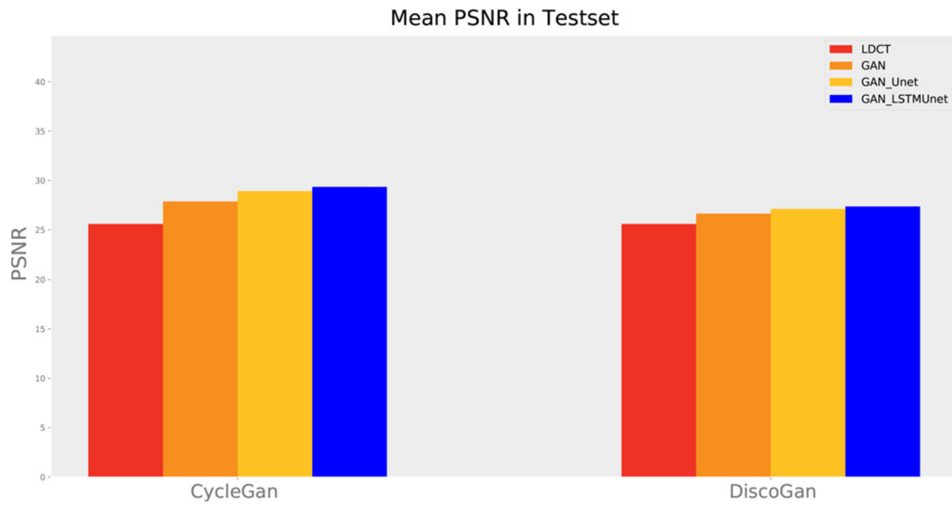

Figure 5. The mean PSNR of denoising GAN with different segmentation settings.

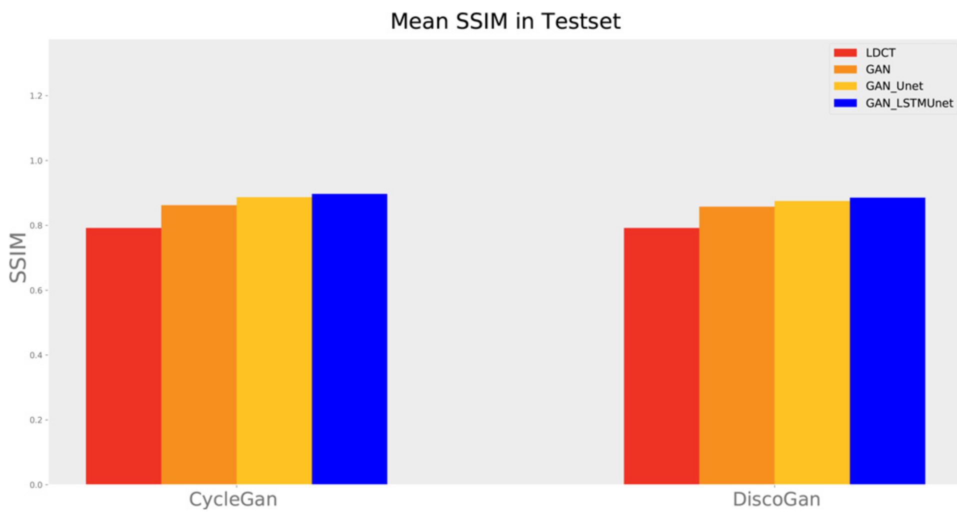

Figure 6. The mean SSIM of denoising GAN with different segmentation settings.

segmentation information as domain knowledge. It is worth to mention that, as we know, in the medical image scenario we can hardly get qualified mask images (e.g. for some specific tasks). However, in our methods, the segmentation networks and denoising networks use different datasets. This means that we can transfer this kind of domain knowledge even from a public available datasets for LDCT denoising.

5.2 *Better Segmentation Makes Better Denoising Performance*

Moreover, as we can see from Figures 5 and 6, the results of our denoising GAN with segmentation information have some trends. Since LSTMUnet has better segmentation performance than normal Unet structure, whether CycleGAN or DiscoGAN denoising structure shows the trends that the better performance the segmentation networks we can use, the better denoising performance we can get. This conclusion works for both PSNR and SSIM metrics. We can also imply that segmentation transfer the domain knowledge even in pixel level.

6. CONCLUSION

We presented a denoising generative adversarial network with segmentation network structure and semantic segmentation information for LDCT denoising. We showed that the segmentation information as domain knowledge can be transferred from mask NDCT images to our denoising GAN to get a better performance on LDCT denoising task. We demonstrated that the more accurate our semantic segmentation model is, the better denoising GAN performance is. Moreover, since the dataset used for semantic segmentation is different from the dataset used for denoising and they are from the same domain (lung CT images), we conclude that this kind of domain knowledge can be shared.

ACKNOWLEDGMENT

This work was supported by Educational Commission of Zhejiang Province of China under grant no. Y202044452.

REFERENCES

[1] J. Liu, J. Ma, Y. Zhang, Y. Chen, J. Yang, H. Shu, L. Luo, G. Coatrieux, W. Yang, Q. Feng, and W. Chen, "Discriminative feature representation to improve projection data inconsistency for low dose ct imaging," IEEE Trans. Med. Imaging **36**, 2499–2509 (2017).

[2] Q. Xu, H. Yu, X. Mou, L. Zhang, J. Hsieh, and G. Wang, "Low-dose X-ray CT reconstruction via dictionary learning," IEEE Trans. Med. Imaging **31**, 1682–1697 (2012).

[3] Y. Zhang, X. Mou, G. Wang, and H. Yu, "Tensor-based dictionary learning for spectral CT reconstruction," IEEE Trans. Med. Imaging **36**, 142–154 (2017).

[4] A. Cheddad, C. Svensson, J. Sharpe, F. Georgsson, and U. Ahlgren, "Image processing assisted algorithms for optical projection tomography," IEEE Trans. Med. Imaging **31**, 1–15 (2012).

[5] Y. Chen, L. Shi, Q. Feng, J. Yang, H. Shu, L. Luo, J.L. Coatrieux, and W. Chen, "Artifact suppressed dictionary learning for low-dose ct image processing," IEEE Trans. Med. Imaging **33**, 2271–2292 (2014).

[6] M. I. Khan, F. X. Aubet, M. O. Pahl, and J. Härri, "Deep learning-aided resource orchestration for vehicular safety communication," *2019 Wireless Days (WD)* (IEEE, Piscataway, NJ, 2019), pp. 1–8.

[7] M. Shamim, A. H. Muneer, and M. Ghulam, "Automatic fruit classification using deep learning for industrial applications," IEEE Trans. Ind. Inform. **15**, 1027–1034 (2019).

[8] S. Bhattacharya, P. K. R. Maddikunta, I. Meenakshisundaram, T. R. Gadekallu, S. Sharma, M. Alkahtani, and M. H. Abidi, "Deep neural networks based approach for battery life prediction," CMC-Comput. Mater. Contin. **69**, 2599–2615 (2021).

[9] C. Iwendi, P. K. R. Maddikunta, T. R. Gadekallu, K. Lakshmanna, A. K. Bashir, and M. J. Piran, "A metaheuristic optimization approach for energy efficiency in the IoT networks," Softw. - Pract. Exp. **51**, 2558–2571 (2021).

[10] C. Feng, K. Yu, M. Aloqaily, M. Alazab, Z. Lv, and S. Mumtaz, "Attribute-based encryption with parallel outsourced decryption for edge intelligent IoV," IEEE Trans. Veh. Technol. **69**, 13784–13795 (2020).

[11] S. Kenji, "Overview of deep learning in medical imaging," Radiol. Phys. Technol. **10**, 257–273 (2017).

[12] E. Klang, "Deep learning and medical imaging," J. Thoracic Dis. **10**, 1325–1328 (2018).

[13] H. Chen, Y. Zhang, M.K. Kalra, F. Lin, Y. Chen, P. Liao, J. Zhou, and G. Wang, "Low-dose CT with a residual encoder–decoder convolutional neural network," IEEE Trans. Med. Imaging **36**, 2524–2535 (2017).

[14] J. M. Wolterink, T. Leiner, M. A. Viergever, and I. Išgum, "Generative adversarial networks for noise reduction in low-dose CT," IEEE Trans. Med. Imaging **36**, 2536–2545 (2017).

[15] Q. Yang, P. Yan, Y. Zhang, H. Yu, Y. Shi, X. Mou, M.K. Kalra, Y. Zhang, L. Sun, and G. Wang, "Low dose CT image denoising using a generative adversarial network with Wsserstein distance and perceptual loss," IEEE Trans. Medical Imaging **37**, 1348–1357 (2018).

[16] M. Ran, J. Hu, Y. Chen, H. Chen, H. Sun, J. Zhou, and Y. Zhang, "Denoising of 3D magnetic resonance images using a residual encoder–decoder Wasserstein generative adversarial network," Med. Image Anal. **55**, 165–180 (2019).

[17] Z. Hong, X. Fan, T. Jiang, and J. Feng, "End-to-end unpaired image denoising with conditional adversarial networks," Proc. AAAI Conf. Artif. Intel. **34**, 4140–4149 (2020).

[18] H. Shan, Y. Zhang, Q. Yang, U. Kruger, M.K. Kalra, L. Sun, W. Cong, and G. Wang, "3D convolutional encoder–decoder network for low-dose CT via transfer learning from a 2D trained network," IEEE Trans. Medical Imaging **37**, 1522–1534 (2018).

[19] W. Yang, H. Zhang, J. Yang, J. Wu, X. Yin, Y. Chen, H. Shu, L. Luo, G. Coatrieux, Z. Gui, and Q. Feng, "Improving low-dose ct image using residual convolutional network," IEEE Access **5**, 24698–24705 (2017).

[20] S. Asgari Taghanaki, K. Abhishek, J. P. Cohen, J. Cohen-Adad, and G. Hamarneh, "Deep semantic segmentation of natural and medical images: A review," Artificial Intelligence Review **54**, 137–178 (2021).

[21] I. Goodfellow, J. Pouget-Abadie, M. Mirza, B. Xu, D. Warde-Farley, S. Ozair, and Y. Bengio, "Generative adversarial nets," Adv. Neural Inform. Process. Syst. **27**, 2672–2680 (2014).

[22] I. Goodfellow, NIPS 2016 tutorial: Generative adversarial networks. arXiv Preprint arXiv:1701.00160 (2016).

[23] J. Zhu, T. Park, P. Isola, and A. A. Efros, "Unpaired image-to-image translation using cycle-consistent adversarial networks," *Int'l. Conf. on Computer Vision (ICCV)* (IEEE, Piscataway, NJ, 2017), pp. 2223–2232.

[24] H. Chen, Y. Zhang, W. Zhang, P. Liao, K. Li, J. Zhou, and G. Wang, "Low-dose CT via convolutional neural network," Biomed. Opt. Express **8**, 679–694.

[25] P. Isola, J. Zhu, T. Zhou, and A. A. Efros, "Image-to-image translation with conditional adversarial networks," *IEEE Conf. on Computer Vision and Pattern Recognition (CVPR)* (IEEE, Piscataway, NJ, 2017).

[26] T. Kim, M. Cha, H. Kim, J. K. Lee, and J. Kim, "Learning to discover cross-domain relations with generative adversarial networks," *Int'l. Conf. on Machine Learning* (2017), pp. 1857–1865, PMLR.

[27] J. Long, E. Shelhamer, and T. Darrell, "Fully convolutional networks for semantic segmentation," *IEEE Conf. on Computer Vision and Pattern Recognition (CVPR)* (IEEE, Piscataway, NJ, 2015), pp. 3431–3440.

[28] V. Badrinarayanan, A. Kendall, and R. C. SegNet, A deep convolutional encoder–decoder architecture for image segmentation. arXiv Preprint arXiv:1511.00561, 5 (2015).

[29] O. Ronneberger, P. Fischer, and T. Brox, "U-Net: Convolutional networks for biomedical image segmentation," *Medical Image Computing and Computer-Assisted Intervention 2015*, LNCS, Vol. 9351 (Springer, Cham, 2015), pp. 234–241.

[30] R. Azad, M. Asadi-Aghbolaghi, M. Fathy, and S. Escalera, "Bi-directional ConvL-STM U-Net with densley connected convolutions," *Int'l. Conf. on Computer Vision Workshop (ICCVW)* (IEEE, Piscataway, NJ, 2019).

[31] A collection of CT images, manually segmented lungs and measurements in 2/3D, http://www.kaggle.com/kmader/finding-lungs-in-ct-data.

[32] Data Science Bowl 2017, http://www.kaggle.com/c/data-science-bowl-2017/data.

[33] X. Yi and P. Babyn, "Sharpness-aware low-dose CT denoising using conditional generative adversarial network," J. Digital Imag. **31**, 655–669 (2018).

[34] F. Chollet, Keras (2015) https://keras.io/.

[35] M. Abadi, A. Agarwal, P. Barham, E. Brevdo, Z. Chen, C. Citro, G.S. Corrado, A. Davis, J. Dean, M. Devin, and S. Ghemawat, TensorFlow: Large-scale machine learning on heterogeneous distributed systems. arXiv Preprint arXiv:1603.04467 (2016).